Evaluation of Multi-layered Graphene Nano-platelet Composite Coatings for Corrosion Control Part I - Contact Potentials and Gas Permeability

C.A.J. Richards*[,a], C.F. Glover[b], G. Williams[a], H.N. McMurray[a], J. Baker[a]

[a] *Materials Research Centre, College of Engineering, Swansea University, Bay Campus, Fabian Way, Swansea, UK, SA1 8EN.*

[b] *Centre of Electrochemical Science and Engineering, University of Virginia, McCormick Avenue, Charlottesville, Virginia, USA, VA22904*

Keywords: Graphene nano-platelets, contact potential, scanning Kelvin probe, oxygen permeability.

*Corresponding author: Tel: 07889271936
E-mail address: 557333@swansea.ac.uk

Abstract

The electronic and diffusion-blocking properties of graphene nano-platelets (GNPs) are quantified with a view to understanding their action as (possible) additives to anti-corrosion coatings. Platelet size and thickness are determined by SEM and BET specific surface area measurements. A Scanning Kelvin probe is used to show that a contact potential of up to 1.4 V develops between GNP particles and various metal substrates: silver, copper, iron and zinc. A novel photochemical method is used to show that oxygen permeation rates through a PVB-GNP (polyvinylbutyral) composite coating decrease by over an order of magnitude as GNP volume fraction increases to 0.056.

1. Introduction

In recent years, graphene has attracted an enormous amount of scientific interest in several areas of research, with many claims associated with its unique physical properties. These include exceptional thermal and electrical conductivity, inherent mechanical strength and an ability to form a robust barrier to the transport of chemical species. These properties arise from the tightly packed 2-dimensional atomic structure of the graphene and sp^2 orbital hybridisation. The structure-property relationships for graphene have been widely reviewed in the relevant literature [1-3].

One area of interest is the use of graphene as a corrosion preventative coating or coating additive for metal surfaces [4-12]. The claims associated with graphene used in this manner fall into two categories: i) graphene acts as an effective barrier to the through coating diffusion of chemical species, thereby reducing the rate of mass transport of corrosion relevant species such as O_2, H_2O and electrolyte ions [1-3,6,10-12], ii) by virtue of its electrical conductivity [1-3], and thus its ability to support electron transfer reactions, graphene may displace electrochemical activity away from the metal surface and into the graphene coating [13]. This would be significant in, for example, cathodic disbondment of a graphene loaded organic coating where the relevant electrochemical process is cathodic oxygen reduction:

$$O_2 + 2e^- + 2H_2O \rightarrow 4OH^- \quad (1)$$

However, it should be noted that making the coating a cathode might have a corrosion accelerating effect where metal is exposed at a coating defect due to coating-defect coupling.

Despite favourable properties, single layer or continuous thin films of graphene have limited feasibility for large scale applications (e.g. protection for metal surfaces) owing to the production costs associated with the deposition methods currently available [14,15]. In response to this, alternative embodiments of graphene have been proposed which demonstrate

graphene-like properties at far lower associated production costs and with easier fabrication. The predominant alternatives discussed within the literature are graphene oxide and graphene nanostructures (e.g. platelets, sheets and ribbons) [16-19]. Graphene nano-platelets (GNP) are potentially attractive alternatives to continuous thin film graphene as they can be produced relatively inexpensively, typically via exfoliation of a graphitic source [16, 20-23]. Some ambiguity does exist as to when a nano-platelet ceases to be considered graphene and whether multi-layered graphite should be considered the more appropriate nomenclature [15,24,25]. Nonetheless, GNPs and similar derivatives have been shown to exhibit properties similar to 2D graphene and are consequently worthy of investigation as possible additives to anti-corrosion coatings [19, 26-31]. For graphene produced by the exfoliation of graphite the single particle conductivity for the in-plane direction is estimated to be of the order 10^3 S m^{-1} [28].

In the current paper, we present a systematic study of a series of composite coatings consisting of a conventional organic polymer (polyvinyl butyral, PVB) in which has been dispersed a varying amount of a GNP pigment. Our aim is to address three matters with respect to the role of the GNP:

i.) do they reduce the rates of corrosion of corrosion driven coating failure?
ii.) to what extent do any beneficial effects derive from reduced rates of through coating mass transport?
iii.) to what extent do any beneficial or detrimental effects derive from the displacement of electrochemical reactions away from the metal surface and into the coating?

In the second part of this paper we study the effect of GNP pigmentation on the kinetics and well defined corrosion-driven coating failure mechanism namely cathodic disbondment. However, here in Part 1 we present a basic physical characterisation of the PVB-GNP composite coatings intended to quantify the effect of GNP pigment content with respect to:

i.) producing electronic conductivity of the PVB-GNP composite coatings

ii.) influencing the ability of a PVB-GNP composite coating to develop a contact potential with a metal substrate, and

iii.) reducing through-coating O_2 permeability in PVB-GNP composite coatings

GNP particle size and the number of graphene layers comprising the individual platelets was estimated by using a combination of scanning electron microscope (SEM) imaging and the Brunauer Emmet Teller (BET) nitrogen adsorption technique. Electronic conductivity of the PVB-GNP composite was estimated using a simple through-coating electrical resistance measurement. The ability of the GNP particles to develop a contact potential when electrically connected to a metal substrate was estimated by using a scanning Kelvin probe (SKP) technique to measure the Volta potential difference becoming established between various metal substrates and the GNP particles.

A variety of methods have been described for the measurement of O_2 permeability in polymer/composite films. These include: i) the "calcium button test" [32], (ii) gas chromatography [33], (iii) differential pressure measurements [34], (iv) fluorescence quenching [35] and (v) O_2 amperometry [36]. However, these typically require specialized apparatus (i-v), a transparent film (i) and/or a relatively large film area (i) and (iii). They can also suffer interference from water vapor (i) or difficulty coping with electrically conducting films (v). For these reasons, we describe a simple measurement based on visible light spectrophotometry and the O_2 oxidation of leucomethylene blue as a means of determining the effect of GNP content of the oxygen permeability of the PVB-GNP composite coatings.

2. Materials and Methods

2.1 Materials

A GNP powder was supplied by Haydale Ltd (U.K). Bare (uncoated) metal coupons of 1mm thickness (silver, copper, iron and zinc) were all purchased from Goodfellow metals at 98-99% purity. Hot-dip-galvanised steel coupons (of 0.7 mm thickness with a ~30 μm zinc/0.2% aluminium metallic coating) were supplied by TATA Steel UK. Polyvinyl butyral (MW 70,000-100,000), methylene blue and ethylenediaminetetraacetic acid (EDTA) were all purchased from Sigma-Aldrich Chemical Co.

2.2 Methods

SEM Imaging:

The GNP powder particles were imaged with a Hitachi SU-70 FEG SEM using an accelerating voltage of 10 kV. Images were also taken of the PVB-GNP coating taken at an accelerating voltage of 30 kV.

BET Measurements

The specific surface area of the GNP powder was measured using a TriStar II 3020 Micrometrics surface analyser, employing the BET nitrogen absorption method. Prior to measurement samples were degassed under vacuum for 24 hours at room temperature.

PVB-GNP Film preparation

The PVB-GNP composite coatings were prepared by dispersing the GNP powder in a 15.5% w/w ethanolic solution of polyvinyl butyral (PVB) with a molecular weight to of 70,000-100,000 Daltons. Powder dispersion was carried out using a DAC 150.1 FVZ-K speed mixer for 1 minute at 3500 rpm. All composite films were produced by bar casting the PVB-GNP dispersion onto the relevant substrate using electrical tape (~145 μm in thickness) as a height guide. Following ethanol evaporation at room temperature, this resulted in a dry film thickness

of ~16 μm (as measured by micrometre screw gauge). The volume fraction (φ_{GNP}) of GNP in the PVB-GNP coating was calculated using:

$$\varphi_{GNP} = \left(1 + \frac{M_{PVB} \cdot \rho_{GNP}}{M_{GNP} \cdot \rho_{PVB}}\right)^{-1} \quad (2)$$

where M_{PVB} is the mass of PVB used in the coating formulation, M_{GNP} the mass of GNP pigment, ρ_{PVB} the density of PVB (~0.8 g cm^{-3}) [37] and ρ_{GNP} is the density of the GNP pigments (~2.25 g cm^{-3}). The value for the supplied GNP pigment was quoted from supplying company literature and is in good agreement with previously published values for GNP density [16].

Through Coating Electrical Conductivity

Through-coating conductivity was measured by sputtering an 8 mm x 9 mm (72 mm^2) area of gold-palladium, of roughly 50 nm in thickness, over a PVB-GNP (0 to 0.056 φ_{GNP}) coated galvanized steel substrate using a Quorum Q150T ES sputtering machine, as shown in Fig. 1. Sputtering of the gold-palladium contact was done to ensure good electrical contact with the PVB-GNP composite surface and to provide a known area for the resulting calculations for conductivity. Electrical resistance was then measured from the sputtered area to the galvanized steel substrate using a 34XR-A Amphrobe multimeter.

Figure 1

Scanning Kelvin probe measurements

The design and operation of the SKP apparatus has been described elsewhere, as has the SKP calibration procedure in terms of electrochemical potential [37]. The SKP reference probe consisted of a gold wire of diameter 125 μm vibrating vertically at 280 Hz with amplitude of 40 μm at 100 μm above the sample surface.

Oxygen Permeation Measurements

A photochemical technique based on the oxygen indictor properties of methylene blue was employed to determine the oxygen permeability of the PVB-GNP films, a detailed description of which is listed in the discussion and results section of this paper. Methylene blue absorbance and hence oxygen permeability was determined photospectrometrically using a Lambda XLS Perkin Elmer UV/Vis spectrophotometer.

3. Results and Discussion

3.1 SEM Imaging

Figure 2

The GNP powder was dispersed in ethanol (~0.1 g/cm^3) and a thin film of the dispersion deposited on to a cleaned galvanized steel substrate using a 1 cm^3 micropipette. This was then allowed to dry in air, leaving the GNP particles weakly adherent to the substrate. Fig. 2 shows an SEM image of the GNP deposited in the above manner. GNP diameters were estimated directly using a graticule and were found to have an average planar diameter of 2.95 μm +/- 2 μm. This relatively broad size distribution is expected of the GNP produced via a plasma ablation route [16, 38,39], the hallmarks of an ablated production route are also evident in the textured cleavage appearance of the platelets. GNP thicknesses were more difficult to estimate using the SEM but, from the measurements taken, lay in the region of 20-200 nm.

Figure 3

The SEM image in Fig. 3 shows the air-facing surface of a typical bar-cast PVB-GNP composite coating with $\varphi_{GNP} = 0.056$. The GNPs which are visible through the PVB matrix are broadly similar in appearance to those in Fig. 2 but show a tendency to orientate and align with the bar-cast drawing direction. Thus, the GNP particles in Fig. 3 tend to exhibit an orientation

in which the platelets are co-planar with coating surface, as compared with the random orientation of the platelets in Fig. 2.

3.1 BET Nitrogen Absorption

Representative curves showing adsorption and desorption of N_2 on GNP powder are shown in Fig. 4. Very little hysteresis is observable, which indicates an absence in mesoporosity and resulting capillary condensation [40]. The absorption measurements were repeated 3 times on separate GNP powder samples. Analysis of the linear region of the BET adsorption isotherms derived from these measurements gave a mean specific surface area of 17 m^2/g (+/- 0.6 m^2/g). The theoretical surface area of single layer graphene has been reported to be roughly 2600 m^2/g [1] and the interlayer spacing of multilayer graphene has been shown to be 0.34 nm [41]. From these quantities, combined with the N_2 BET specific area for our GNP sample we can calculate a mean platelet thickness of 155 nm (+/- 5.5 nm) or ~53 layers of graphene. This thickness estimate is consistent with the rough estimate of 20-200 nm taken from the SEM image in Fig. 2.

Figure 4

3.2 Through-Coating Conductivity:

Coating conductivity was calculated using equation (3):

$$k = \frac{d}{R.A} \tag{3}$$

where k is the conductivity (Sm^{-1}), R the measured resistance (Ω), A is the area of the sputtered contact (m^2) and d the film thickness (m). A resistance measurement of 150 Ω (+/- 5 Ω) was recorded for a 16 μm thick coating PVB-GNP composite coating with a pigment volume fraction of 0.056 φ_{GNP}. The sputtered contact area was 0.72 cm^2 and the conductivity was calculated to be 1.48 x 10^{-5} S m^{-1} (+/- 0.5 x 10^{-5} S m^{-1}). PVB-GNP coatings with $\varphi_{GNP} \leq 0.028$

were highly resistive and no reliable conductivity measurement could be performed with the apparatus described. PVB-GNP coatings with $\varphi_{GNP} > 0.06$ were very brittle and were not characterised further. Nevertheless, these findings imply that GNP particle-particle contact in the PVB-GNP coating can be sufficient to allow electronic conduction, albeit rather inefficiently with low coating conductivity.

3.3 Volta potential measurements

Various types of Volta potential measurement were carried out using the SKP technique. The first was aimed at measuring any contact potential [42] becoming established between GNP particles and a metal substrate with which they were in electrical contact. This involved bar casting an ethanolic dispersion (~0.1 g/cm^3) of the GNP powder onto metallic coupons of varying work function – namely; silver, copper, iron and zinc. Prior to deposition, all the metal coupons were polished to a 1200 μm grit finish using emery paper. Scotch tape of 120 μm thickness was used as a height guide when depositing the dispersion, which was then allowed to dry in air. An approximate dry GNP powder deposit of thickness ~6 μm could then be calculated using the respective densities of the GNP and ethanol (~2.2 g/cm^3 and 0.8 g/cm^3). The SKP was used to scan from the polished (bare) metal surface to the GNP covered surface for each coupon. The potentials recorded by the SKP were equal to the Volta potential difference between the sample surface and the gold SKP tip ($\Delta\Psi^{sample}_{gold}$). Volta potential profiles were recorded by scanning over a 6 mm distance at hourly intervals for a 12-hour period in room air at 50% RH and at 20°C. A schematic representation of the sample set-up and measurements is shown below in Fig. 5.

Figure 5

Volta potential ($\Delta\Psi^{sample}_{gold}$) profiles, obtained as above, are shown in Fig. 6 for the various metal substrates. The data in Fig. 6 are explicable on the basis of a contact potential

being established between the metal substrate and the overlying GNP particles as a consequence of the work function difference which exists between the graphene and relevant metal. When two (dissimilar) metals (or electronic conductors) with differing work functions (W_1 and W_2) are connected in such a way that electrons can flow freely from one to another (so that they share a common Fermi level) a Volta potential difference (or contact potential) becomes established between metal 1 and metal 2 such that [42]:

$$\Delta\Psi_1^2\,(\text{eV}) = W_1 - W_2 \tag{4}$$

Figure 6

Given the above, the data in Fig. 6 may be analysed in terms of the various 'metal – gold' contact potentials ($\Delta\Psi^{\text{metal}}_{\text{gold}}$) together with the corresponding GNP-metal contact potentials ($\Delta\Psi^{\text{GNP}}_{\text{metal}}$). The quantities $\Delta\Psi^{\text{metal}}_{\text{gold}}$ are obtained directly from the left-hand side of Fig. 6 (bare metal) whereas the quantities $\Delta\Psi^{\text{GNP}}_{\text{metal}}$ are obtained from the difference in $\Delta\Psi$ (step height in $\Delta\Psi$ profile) between the LHS (bare metal) and RHS (GNP on metal) of Fig. 6.

Material	W (eV) (Photoelectric)	$\Delta\Psi_{Gold}^{Metal}$ Calculated (V)	$\Delta\Psi_{Gold}^{Metal}$ Measured (V)
Carbon/GNP	5.0[43]	0.1	0.62(i)
Silver	4.72[44]	-0.38	-0.23
Copper	4.65[43]	-0.45	-0.55
Iron	4.5[43]	-0.6	-0.70
Zinc	4.33[43]	-0.77	-1.20
Gold	5.1[43]	0	-

Table 1: Literature values for each relevant metal along with carbon, also expressed in relation to the potential for gold and alongside the Volta potential values determined using the ambient SKP experiment. Where (i) represents the value for the GNP extrapolated from the intercept of Fig. 7.

Wherever possible we have used the literature work function values reported for polycrystalline metal samples as this best reflects the condition of the metal coupons used in our experiments. However, the literature value reported for polycrystalline silver (4.26 eV) was obtained using a thin silver film epitaxially deposited on a quartz substrate and is significantly lower than the values reported for bulk silver crystals [43,44]. For this reason, we have used the literature value for bulk and annealed silver [44] as this better represents the condition of the supplied silver coupon used. It should be noted that the presence of an oxide layer and/or the presence of trace adsorbed contamination can all act to change metallic work functions by up to 0.2 eV[45,46]. Nevertheless, a reasonable degree of agreement exists between our measured $\Delta\Psi^{metal}_{gold}$ values and those which may be calculated from literature values of metallic work functions using equation (4) – as shown in table 1. Furthermore, if we are correct in interpreting the varying step-height of the $\Delta\Psi$ profiles in Fig. 6 in terms of a metal-GNP contact potential, the following should be true:

$$\Delta\Psi^{GNP}_{metal} = \Delta\Psi^{GNP}_{gold} - \Delta\Psi^{metal}_{gold} \qquad (5)$$

So that a plot of the $\Delta\Psi^{GNP}_{metal}$ vs $\Delta\Psi^{metal}_{gold}$ should have a slope of -1 and an intercept equal to $\Delta\Psi^{GNP}_{gold}$. The resulting plot shown in Fig. 7 is a good straight line with a correlation coefficient of 0.93, a slope of -0.89 and an intercept of 0.62 V. The measured and theoretical slope of Fig. 7 (-0.89 vs -1) are in good agreement. The value of $\Delta\Psi^{GNP}_{gold}$ obtained from the y-intercept of Fig. 7 is 0.62 V (+/-0.01 V). From this value, using equation (4) and W_{gold} = 5.1 eV[43], we can calculate a W_{GNP} value of 5 eV (+/- 0.1 eV). This again is in reasonable agreement with previous published estimates of 5 eV [43] for carbon.

Figure 7

3.4 Oxygen Permeation

Oster and Wotherspoon et al demonstrated an effective method of photoreducing MB using intense white light in conjunction with (EDTA) as the sacrificial reducing agent [47]. The colorless leucomethylene blue (LMB) thus formed can undergo a rapid and stoichiometric re-oxidation to MB per equation (6) [48,49].

$$2LMB + O_2 \rightarrow 2MB^+ + 2\mathrm{OH} \quad (6)$$

LMB re-oxidation kinetics have been studied as a function of pH and it has been shown that re-oxidation is fastest at high pH (9.6) where the relevant species is probably the LMB anion (LMB^-) [50]. Under these conditions the pseudo first order rate constant for LMB re-oxidation in air-saturated water is 89 M^{-1} s^{-1}. Chemical stability of the MB/LMB system has been demonstrated over 150 photoreduction – air oxidation cycles without apparent degradation of the dye [51].

For the method used in this paper, a quartz cuvette was filled with a solution of 2 x10^{-5} M aqueous MB and 1 x 10^{-3} M aqueous EDTA adjusted to pH 10 using aqueous NaOH. A free-standing PVB film containing the relevant volume fraction φ_{GNP} was then sealed over the cuvette mouth using a two-part epoxy (Loctite® - Double Bubble). A Schematic illustration of the sample cell is shown in Fig. 8. All sample preparation was carried out in a nitrogen atmosphere (nitrogen glovebox) and any residual dissolved oxygen was reduced by repeatedly photo-bleaching the MB using a xenon arc lamp until it became and remained completely colourless. Photoreduction of methylene blue can occur (slowly) when exposed to ambient light and the cuvette was therefore sealed away from external light sources throughout any subsequent measurement of LMB reoxidation rate.

Figure 7

The time-dependent concentration of MB (Extinction Coefficient 73,004 L mol^{-1} cm^{-1} at λ_{max} 662 nm [52]), was determined spectrophotometrically immediately following

photoreduction (when it is approximately zero) and at 15 minute intervals thereafter for a period of 1 hour. Immediately before each spectrophotometric measurement the cuvette was vigorously shaken to allow any oxygen permeating through the PVB-GNP film to react through reaction (6). A baseline LMB reoxidation rate was obtained using an impermeable glass slide in the place of the PVB-GNP film with the aim of estimating the rate of any O_2 ingress through the epoxy seal. Two GNP pigment volume fractions were chosen, 0.056 φ_{GNP} and 0.028 φ_{GNP}, as well as an unpigmented PVB sample.

Figure 9

Fig. 9 shows the time-dependent MB absorbance produced by O_2 permeation through each of the PVB-GNP films. From these measurements rate of change in MB concentration may be calculated using a derivation of the Beer Lambert Law:

$$\frac{dc}{dt} = \frac{dA}{dt} \times \frac{l}{\varepsilon} \qquad (7)$$

where A is Absorbance, t is time (seconds) □ is Extinction Coefficient (mol^{-1} dm^3 cm^{-1}), *c* is concentration (mol L^{-1}) and □ is the optical path length (1 cm in our experiments).

From this and knowing the stoichiometry of reaction between leuco methylene blue (LMB) and oxygen eq. (3) we can calculate oxygen permeability as follows:

$$O_2 \text{ permeability} = \frac{dA}{dt} \times \left(\frac{vol.\ of\ MB\ sol.}{2 \cdot \varepsilon}\right) \times \left(\frac{film\ thickness}{film\ area}\right) \div (0.2 \times 101325) \qquad (8)$$

where O_2 permeability is in units of mol s^{-1} m^{-1} Pa^{-1}, film thickness and area are in m and m^2, respectively, and the atmospheric partial pressure of O_2 is given by 0.2 x 101325 in Pa. Note, it is implicit in the derivation of equation (x) that the partial pressure of O_2 inside the experimental cuvette is kept ~zero at all times through reaction (3) so that the O_2 partial

pressure difference across the measured PVB-GNP films is equal to the O_2 partial pressure in the external (air) atmosphere.

Figure 10

Fig. 10 is a plot of the calculated O_2 permeation values against the respective φ_{GNP}. The O_2 permeation coefficient for an unpigmented PVB film was calculated as 1.01 x 10^{-16} mol s^{-1} m^{-1} Pa^{-1} and for the 0.028 and 0.056 φ_{GNP} PVB-GNP films were calculated as 3.60 x 10^{-17} and 5.99 x 10^{-18} mol s^{-1} m^{-1} Pa^{-1}, respectively. These values support the hypothesis of the GNP pigment decreasing the permeability of the composite coating: at a pigment volume fraction of 0.056 φ_{GNP} the permeation coefficient is almost two orders of magnitude lower than that of an unpigmented PVB system. The longitudinal alignment of the platelets, shown in the SEM image of the PVB-GNP composite in Fig. 3, could certainly act to retard the through coating diffusion of electroactive species (in this case O_2) to the metal surface by increasing the tortuosity of the associated coating. These findings agree with what has been reported within the literature with regards to graphene and GNPs (and similar graphene derivatives) being robust barriers to the permeation of corrosion relevant species [4,6,10-12,22].

4. Conclusions

When GNP particles are brought into physical contact with a range of non-noble metal substrates the electrical conduction pathways existing between the GNPs and the underlying (oxide covered) metal surface are sufficiently to allow the development of a contact potential the value of which consistent with differences in tabulated values of electronic work function for the respective materials. Thus, a contact potential difference of ~1.2 V is measured for GNPs deposited on a zinc substrate, whereas a value of ~0.6 V is measured for the GNPs deposited on iron. The magnitude and polarity of these contact potentials (GNP is always noble of the metal) is such that they are predicted to displace the cathodic reduction reactions

associated with metallic corrosion (such as oxygen reduction) away from the metal surface. That is to say, the GNPs could form a galvanic couple with the metal in which the GNP acts as the cathode.

When GNPs are dispersed in a non-conducting, film forming polymer (PVB) the resulting PVB-GNP composite coatings show evidence of through-coating electronic conduction arising from GNP particle-particle electron percolation. The resulting bulk conductivities are low and were only measurable (1.48×10^{-5} S m^{-1}) for the highest experimental GNP volume fractions (0.056). Nevertheless, it is reasonable to expect that metal-GNP contact potentials will develop at the interface between a metallic substrate and a GNP-polymer composite coating and that this contact potential could also influence the location of electrochemical reactions as outlined above.

When the diffusion rate of oxygen (O_2) is measured across free-standing PVB-GNP films the O_2 permeability decreases monotonically with increasing GNP volume fraction. The O_2 permeability of films containing 0.056 volume fraction GNP was measured to be 2 orders of magnitude lower than that of pure PVB. These changes in permeability probably arise as a consequence of the GNP particles themselves being impermeable to O_2 and the high aspect ratio of the particles forcing O_2 to diffuse via a tortuous path through the composite films. Again, the O_2 blocking effect of GNP addition could reasonably be expected to retard the rate of corrosion reactions where the through-coating transport of O_2 is a rate controlling process. Reduced permeability in through-coating diffusion of electroactive species, namely oxygen, is possible due to increased tortuosity of molecular pathways by the platelets. When GNP is added to an organic coating system at pigment volume fractions of ≥ 0.028 φ_{GNP} there is a significant reduction in permeated oxygen compared to an unpigmented system.

5. Acknowledgements

The authors recognise the EPSRC, Welsh Government and Tata Steel UK for financial support of this work and Innovate UK for the SPECIFIC Innovation and Knowledge Centre (grant numbers EP/I019278/1, EP/K000292/1, EP/L010372/1). The authors would also like to thank Haydale Ltd for providing materials.

The raw/processed data required to reproduce these findings cannot be shared at this time due to technical or time limitations.

6. References

[1] C. N. R. Rao, A. K Sood, K. S. Subrahmanyam & A. Govindaraj, Graphene: The new two-dimensional nanomaterial. Angewandte Chemie - International Edition, (2009) 48(42), 7752–7777.
[2] Y. Zhu, S. Murali, W. Cai, X. Li, J. W. Suk, J. R. Potts, & R. S. Ruoff. (2010) Graphene and graphene oxide: Synthesis, properties, and applications. Advanced Materials, 22(35), 3906–3924.
[3] M. J. Allen, V. C. Tung, & R. B. Kaner, Honeycomb carbon: A review of graphene. Chemical Reviews, (2010) 110(1), 132–145.
[4] N. T. Kirkland, T. Schiller, N. Medhekar, & N. Birbilis, Exploring graphene as a corrosion protection barrier. Corrosion Science, (2012) 56, 1–4.
[5] A. Gergely, T. & Kristof, Corrosion protection with ultrathin graphene coatings: A review. Hungarian Journal of Industry and Chemistry, (2013) 41(2), 83–108
[6] S. Bohm, Graphene against corrosion. Nature Nanotechnology, (2014) 9(10), 741–742.
[7] J. C. Tuberquia, , Harl, R. R., Jennings, G. KaPrasai, D., & Bolotin, K. I. Graphene: Corrosion-inhibiting coating. ACS Nano, (2012). 6(2), 1102–1108.
[8] B.R. V Dennis, L.T. Viyannalage, V. Anil, Nanocomposite Coatings for Protecting Low-Alloy Steels From Corrosion, Am. Ceram. Soc. Bull. 92 (2013) 18–24.
[9] M. Williams, K. Seunarine, R. Gibbs, C. Spacie, Plasma modification of graphene and graphene like materials for component performance enhancement, Nano Res. 27 (2013) 23–27.
[10] K.C. Chang, M.H. Hsu, H.I. Lu, M.C. Lai, P.J. Liu, C.H. Hsu, et al., Room-temperature cured hydrophobic epoxy/graphene composites as corrosion inhibitor for cold-rolled steel, Carbon N. Y. 66 (2014) 144–153.
[11] M. Yi, Z. Shen, X. Zhao, L. Liu, S. Liang, X. Zhang, Exploring few-layer graphene and graphene oxide as fillers to enhance the oxygen-atom corrosion resistance of composites., Phys. Chem. Chem. Phys. 16 (2014) 11162–7.
[12] D. Prasai, J.C. Tuberquia, R.R. Harl, G.K. Jennings, B.R. Rogers, K.I. Bolotin, Graphene: corrosion-inhibiting coating., ACS Nano. 6 (2012) 1102–8.
[13] K. R. Ratinac, W. Yang, J.J. Gooding, P. Thordarson, F. & Braet, Graphene and related materials in electrochemical sensing. Electroanalysis, (2011) 23(4), 803–826.
[14] R. M. Frazier, W. L. Hough, N. Chopra, K. W. Hathcock. Advances in Graphene-Related Technologies: Synthesis, Devices and Outlook, Recent Patents on Nanotechnology, 2012, Volume 6, Issue 2 , (79 – 98)
[15] K. S. Novoselov, V. I. Fal, , Colombo, L., Gellert, P. R., Schwab, M. G., & Kim, K. REVIEW A roadmap for graphene. Nature, (2012) 490(7419), 192–200.

[16] A. Nieto, D. Lahiri, & A. Agarwal, Synthesis and properties of bulk graphene nanoplatelets consolidated by spark plasma sintering. Carbon, (2012) 50(11), 4068–4077.
[17] P. Taylor, W. Choi, I. Lahiri, R. Seelaboyina, Y.S. Kang, W. Choi, I. Lahiri, R. Seelaboyina, Critical Reviews in Solid State and Materials Sciences Synthesis of Graphene and Its Applications: A Review Synthesis of Graphene and Its Applications: A Review, (2010) 37–41.
[18] M. Xu, T. Liang, M. Shi, & H. Chen, Graphene-Like Two-Dimensional Materials, (2013) Chem. Rev. 2013, 113, 3766−3798
[19] D. R. Dreyer, S. Park, W. Bielawski, & R. S. Ruoff, The chemistry of graphene oxide. Chem.Soc.Rev., (2010) 39, 228–240
[20] Y. Geng, S. J. Wang, & J. Kim, Journal of Colloid and Interface Science, Preparation of graphite nanoplatelets and graphene sheets. Journal of Colloid And Interface Science, (2009). 336(2), 592–598.
[21] G. Wang, J. Yang, J. Park, X. Gou, B. Wang, H. Liu, & J. Yao, Facile Synthesis and Characterization of Graphene Nanosheets, (2008) 8192–8195.
[22] A. Kausar, Z. Anwar, & B Muhammad, Recent Developments in Epoxy / Graphite , Epoxy / Graphene and Epoxy / Graphene Nanoplatelet Composites : A Comparative Review, Polymer-Plastics Technology and Engineering, (2016) 2559
[23] R. Jan, A. Habib, Z.M. Khan, M.B. Khan, M. Anas, A. Nasir, S. Nauman, Liquid exfoliated graphene smart layer for structural health monitoring of composites, 28 (2017) 1565–1574.
[24] A. Bianco, H. M. Cheng, T. Enoki, Y. Gogotsi, R. H. Hurt, N. Koratkar, J. Zhang, All in the graphene family – A recommended nomenclature for two-dimensional carbon materials. Carbon, (2013). 65(Supplement C), 1–6.
[25] P. Wick, A. E. Louw-gaume, M. Kucki, H. F. Krug, K. Kostarelos, B. Fadeel, A.Bianco, Classification Framework for Graphene-Based Materials, (2014) 7714–7718.
[26] B. Roman-Manso, E. Domingues, F. M. Figueiredo, M. Belmonte, & P. Miranzo, Enhanced electrical conductivity of silicon carbide ceramics by addition of graphene nanoplatelets. Journal of the European Ceramic Society, (2015) 35(10), 2723–2731.
[27] B. Ramezanzadeh, M. H. M. Moghadam, N. Shohani, & M. Mahdavian, Effects of highly crystalline and conductive polyaniline / graphene oxide composites on the corrosion protection performance of a zinc-rich epoxy coating. Chemical Engineering Journal, (2017) 320, 363–375.
[28] B. Marinho, M. Ghislandi, E. Tkalya, C. E. Koning and G. de With, Electrical conductivity of compacts of graphene, multi-wall carbon nanotubes, carbon black and graphite powder, Powder Technology, 221, (2012), 351-328
[29] K. Jeyasubramanian, A. V. Scientist-sf, & R. Ghosh, Corrosion resistance behaviour of graphene / polyvinyl alcohol nanocomposite coating for aluminium-2219 alloy. Journal of Alloys and Compounds, (2017) 716, 259–269.
[30] M. Li, In situ preparation of graphene / polypyrrole nanocomposite via electrochemical co-deposition methodology for anti-corrosion application. Journal of Materials Science, (2017) 52(20), 12251–12265.
[31] B. Ramezanzadeh, A. Ahmadi, & M. Mahdavian, Enhancement of the corrosion protection performance and cathodic delamination resistance of epoxy coating through treatment of steel substrate by a novel nanometric sol-gel based silane composite film filled with functionalized graphene oxide nanosheets. Evaluation and Program Planning, (2016) 109, 182–205.
[32] R. Paetzold, A. Winnacker, D. Henseler, V. Cesari, & K. Heuser, K. Permeation rate measurements by electrical analysis of calcium corrosion Permeation rate measurements by electrical analysis of calcium corrosion, Review of Scientific Instruments (2003) 74, 5147

[33] K. Broka & P. Ekdunge. Oxygen and hydrogen permeation properties and water uptake of Nafion 117 membrane and recast film for PEM fuel cell, Journal of Applied Electrochemistry 27 (1997) 117-123
[34] S. A. Stern, P.J. Gareis, T.F. Sinclair & P.H. Mohr. Performance of a Versatile Variable-Volume Permeability Cell. Comparison of Gas Permeability Measurements…, Journal of Applied Polymer Science, (1963) Vol. 7, pp. 2035-2051
[35] W. Kozak. Application of Fluorescence in measuring oxygen concentration in packages, CHEMIK 2011, 65, 7, 627-632
[36] A. Q. Pham & S. Glass. Characteristics of Amperometric Oxygen Sensor, J. Elecrtorchem. Soc., Vol. 144, No. 11 (1997)
[37] H. N. McMurray, D. Williams, G. Williams & D.A. Worsley, Inhibitor pretreatment synergies demonstrated using a scanning Kelvin probe technique, Corros. Eng. Sci. Technol. 38 (2003) 112–118.
[38] B. K. Jiang, J. Li, & J. Liu, Spark Plasma Sintering and Characterization of Graphene Platelet / Ceramic Composites, (2015). (5).
[39] H. Lee, M. A. Bratescu, T. Ueno, & N. Saito, RSC Advances graphite electrodes. RSC Advances, (2014) 4, 51758–51765.
[40] K. S. W. Sing, D.H Everett, R. A. W. Haul, L. Moscou, R. A. Pierotti, J. Rouquerol, T. Siemieniewska. Pure & Appl. Chem., Vol. 57, 1985 No. 4, pp. 604-619,
[41] P. Wang, J. Zhang, L. Dong, C. Sun, X. Zhao, Y. Ruan & H. Lu, Interlayer Polymerization in Chemically Expanded Graphite for Preparation of Highly Conductive, Mechanically Strong Polymer Composites, Chem. Mater. 2017, 29, 3412−3422
[42] B. Voigtländer, Scanning Probe Microscopy, NanoScience and Technology, 9.4 Contact Potential - pp 129
[43] H. B. Michaelson, The work function of the elements and its periodicity, J. Appl. Phys. (1977), 48, 4729.
[44] A. W. Dweydari and C. H. Mee, Work Function Measurements on (100) and (110) Surfaces of Silver, phys. stat. sol. (a) 27, 223 (1975),
[45] M. Uebel, A. Vimalanandan, A. Laaboudi, S. Evers, M. Stratmann D. Diesing, and M. Rohwerder, Fabrication of Robust Reference Tips and Reference Electrodes for Kelvin Probe Applications in Changing Atmospheres, Langmuir 2017, 33, 10807-10817
[46] R. Hausbrand, M. Stratmann & M. Rohwerder, The Physical Meaning of Electrode Potentials at Metal Surfaces and Polymer/Metal Interfaces: Consequences for Delamination, J. Electrochem. Soc. 155 (7) (2008) C369-C379
[47] G. Ensell, Photoreduction of Methylene Blue by Ethylenediaminetetraacetic. Journal of the American Chemical Society, 157(1954), 7–9.
[48] A. Mills, K. Lawrie, J. Bardin, A. Apedaile, A. Skinner, & C. O. Rourke, An O_2 smart plastic film for packaging, Analyst, 2012, 137, 106 -112
[49] X. Wang, & O. S. Wolfbeis, Optical methods for sensing and imaging oxygen: materials, spectroscopies and applications, Chem. Soc. Rev., 2014, 43, 3666
[50] O. Impert, P. Kita, A. Mills, A. Pietkiewicz-graczyk, & G. Wrzeszcz, G. Kinetics and mechanism of a fast leuco-Methylene Blue oxidation by copper (II)– halide species in acidic aqueous media, Dalton Trans., 2003, 0, 348-353
[51] P. A. Hamlin, & J. L. Lambert, (1971). Determination of Dissolved Oxygen Using Photoreduced Leuco Phenothiazine Dyes, 1970–1972. 43 (4).
[52] K. Basavaiah, U.R. Anil Kumar, K. Tharpa, K.B. Vinay, Validated spectrophotometric methods for the determination of raloxifene hydrochloride in pharmaceuticals, J. Chil. Chem. Soc. 53 (2008) 1635–1639

7. Figures

Fig. 1 Schematic representation of the through-coating conductivity measurement technique.
Fig. 2 Scanning electron microscope image of the GNP deposited from an ethanolic solution and allowed to air dry.
Fig. 3 Scanning electron microscope image of the PVB-GNP composite film (0.056 φ_{GNP}) cast onto a hot dip galvanised steel substrate.
Fig. 4 Nitrogen adsorption isotherm of the GNP powder taken at 77K.
Fig. 5 Schematic representation of the sample set-up and measurements taken for the bare metal and GNP pigment experiment.
Fig. 6. Plots of $\Delta\Psi^{sample}_{gold}$ profiles vs. scan distance measured on silver, copper, iron and zinc substrates where the Volta potential measurements transition from the bare metal surface to a GNP deposited region for each of the metal samples.
Fig. 7 Plot of $\Delta\Psi^{GNP}_{metal}$ vs $\Delta\Psi^{metal}_{gold}$ measured on silver, copper, iron and zinc.
Fig. 8 Schematic illustration of the sample cell for the oxygen permeation experiments.
Fig. 9 A plot of the measured change in absorbance for the photoreduced methylene solutions as a function of φ_{GNP} measured over the course of 1 hour.
Fig. 10 Calculated oxygen permeation coefficients plotted against φ_{GNP} for the unpigmented and each of the PVB-GNP composite coatings measured.

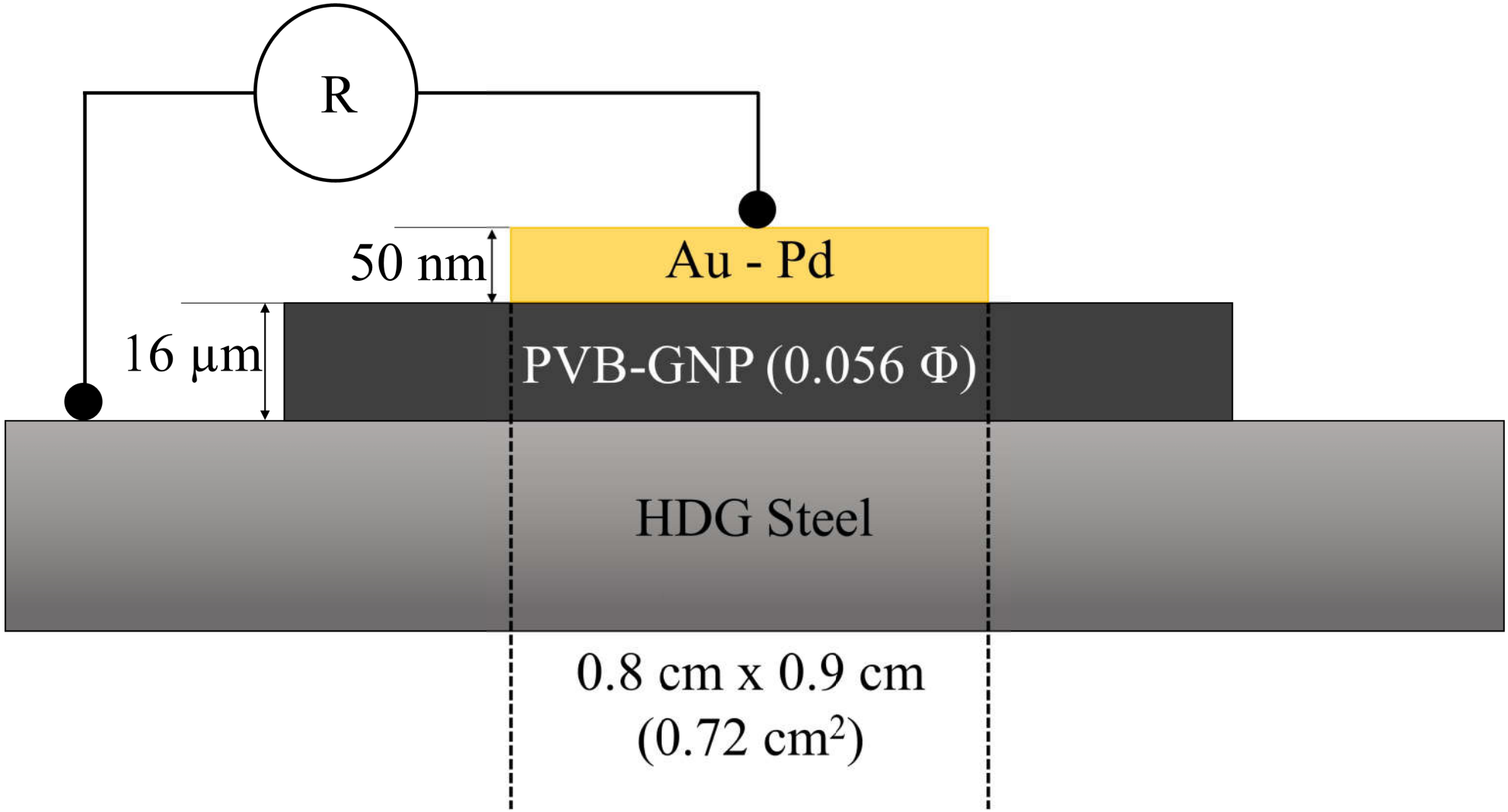
R
50 nm
Au - Pd
16 µm
PVB-GNP (0.056 Φ)
HDG Steel
0.8 cm x 0.9 cm
(0.72 cm²)

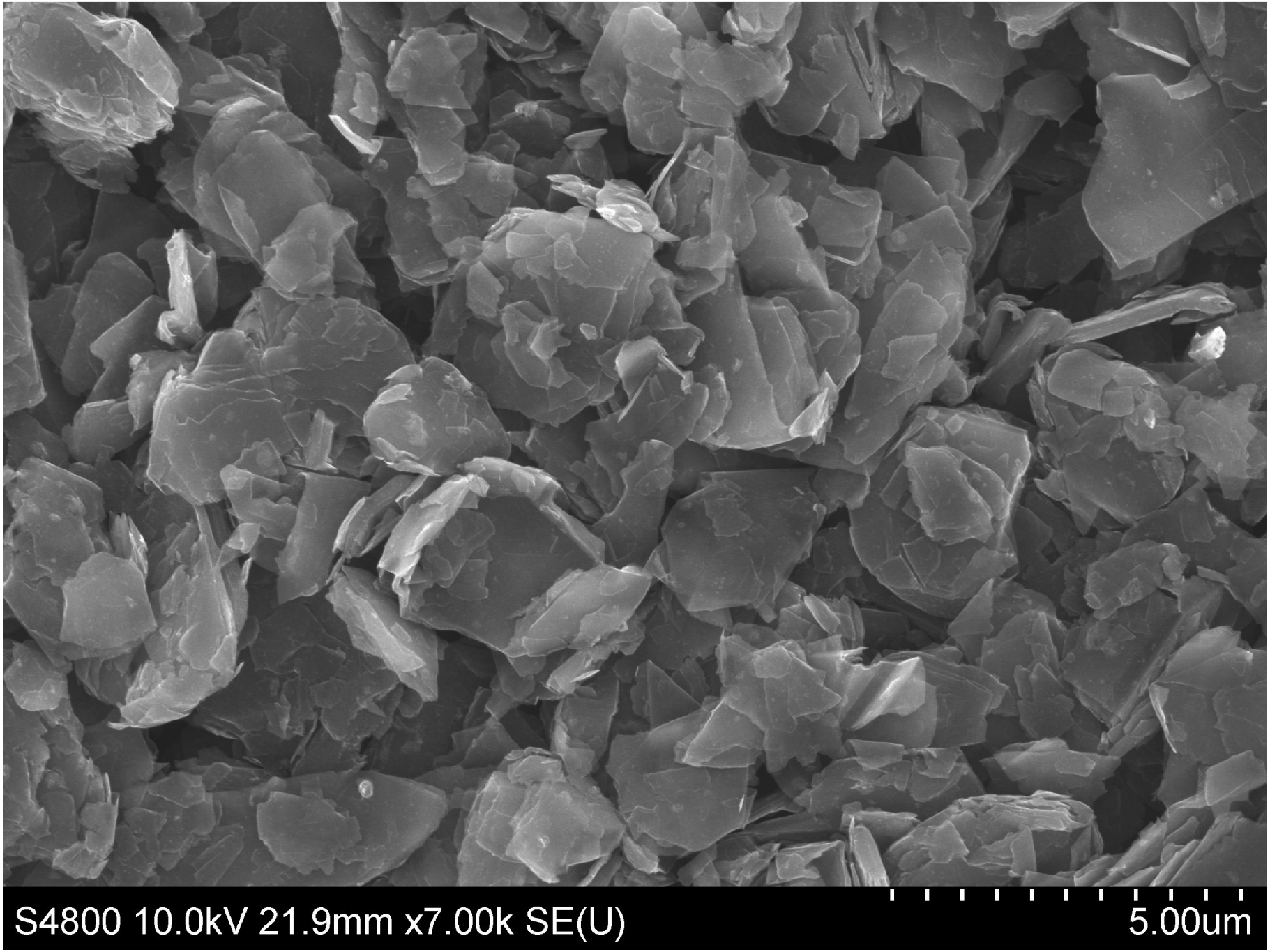
S4800 10.0kV 21.9mm x7.00k SE(U)
5.00um

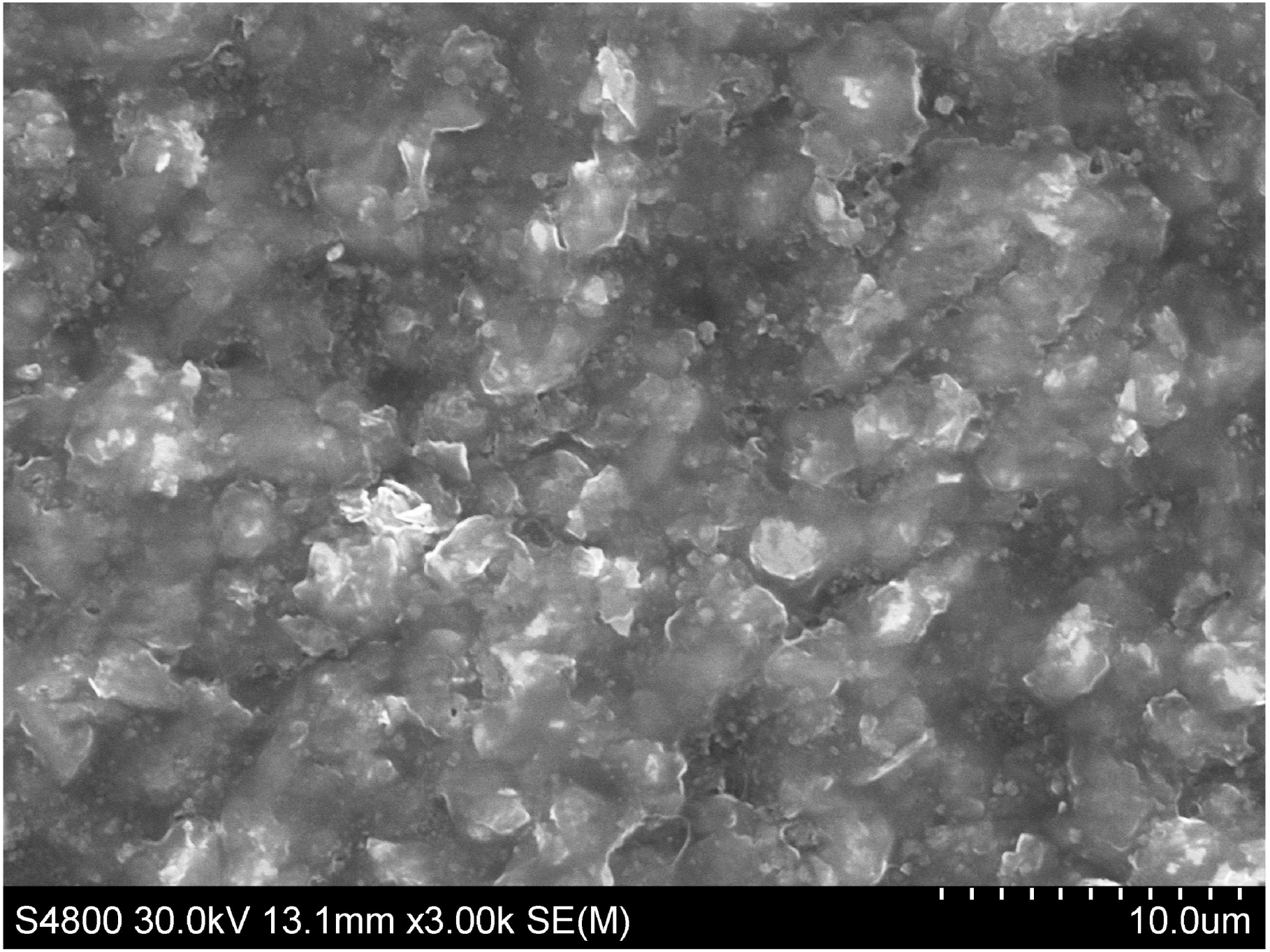
S4800 30.0kV 13.1mm x3.00k SE(M)
10.0um

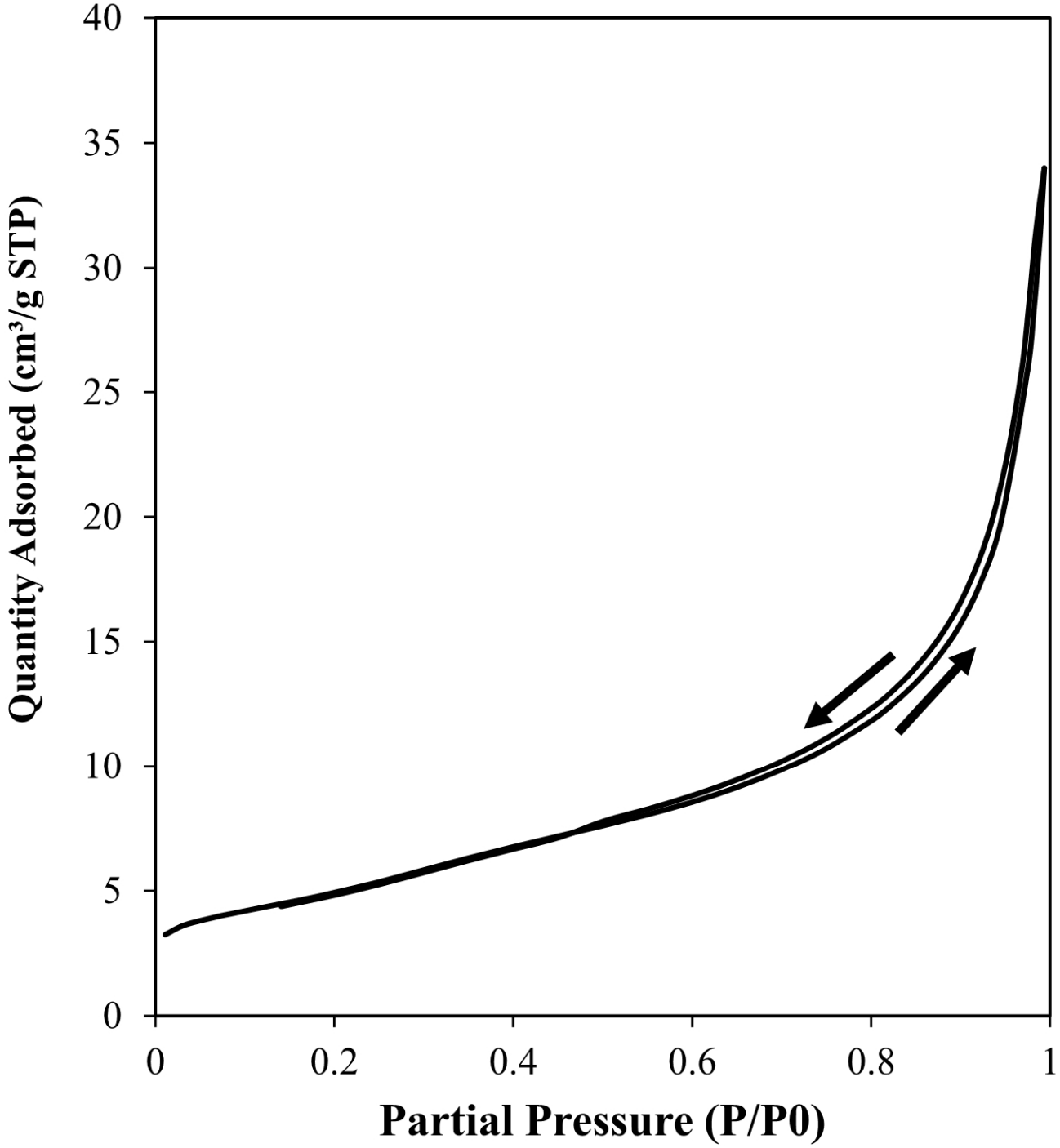
Quantity Adsorbed (cm³/g STP)
40
35
30
25
20
15
10
5
0
0
0.2
0.4
0.6
0.8
1
Partial Pressure (P/P0)

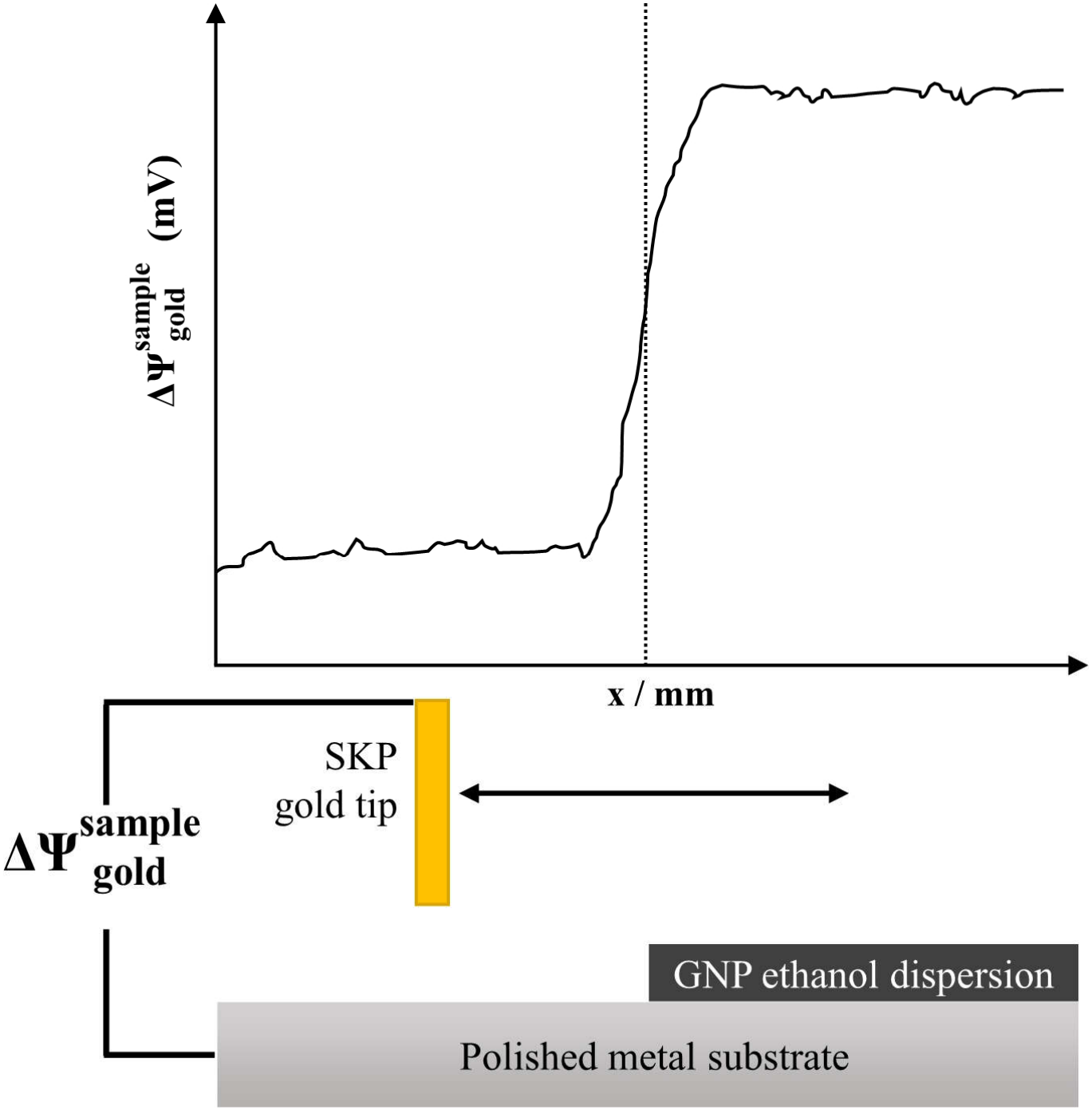
$\Delta\Psi^{sample}_{gold}$ (mV)
x / mm
SKP
gold tip
$\Delta\Psi^{sample}_{gold}$
GNP ethanol dispersion
Polished metal substrate

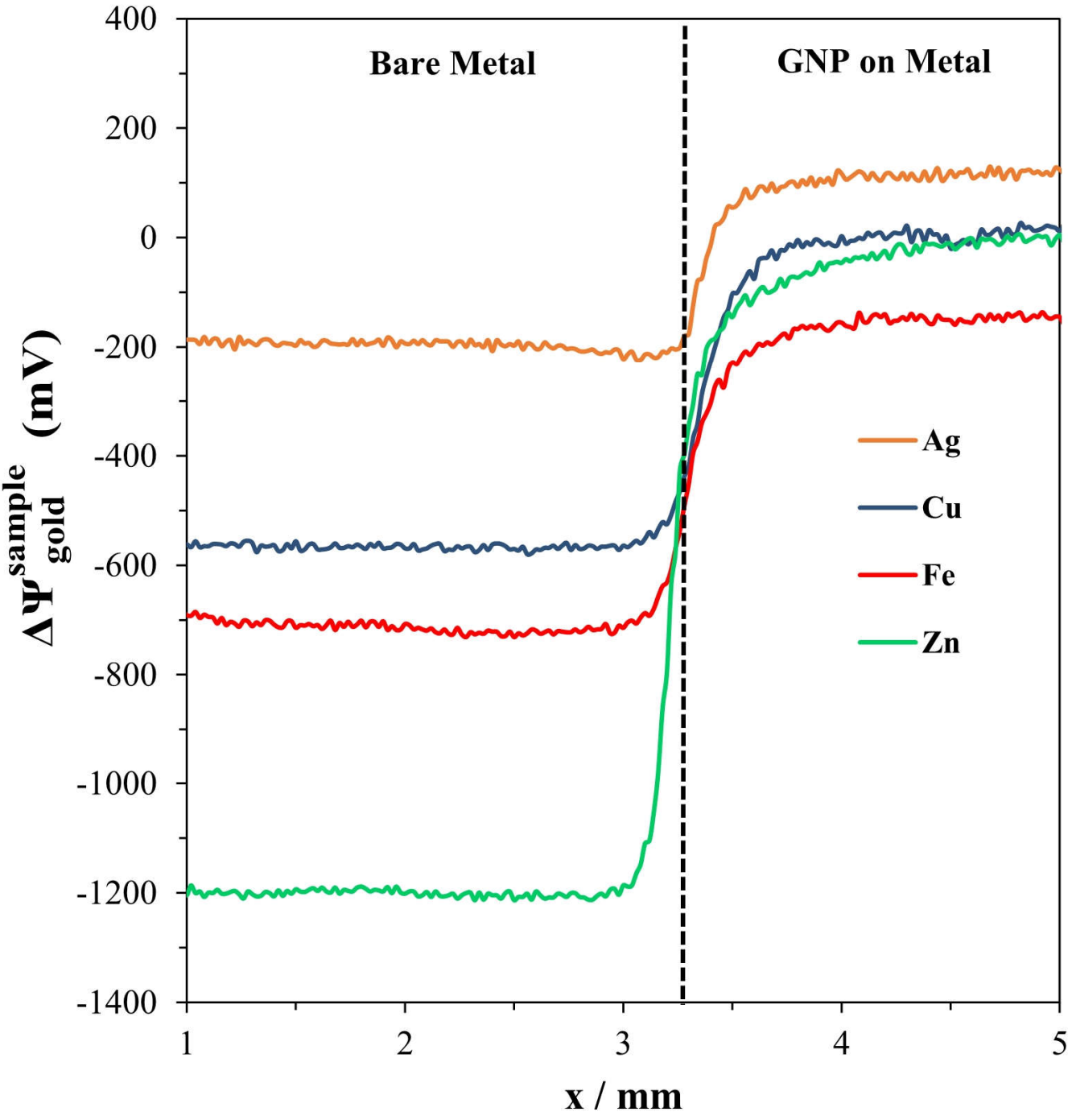
Bare Metal
GNP on Metal
Ag
Cu
Fe
Zn
400
200
0
-200
-400
-600
-800
-1000
-1200
-1400
1
2
3
4
5
x / mm
$\Delta\Psi^{sample}_{gold}$ (mV)

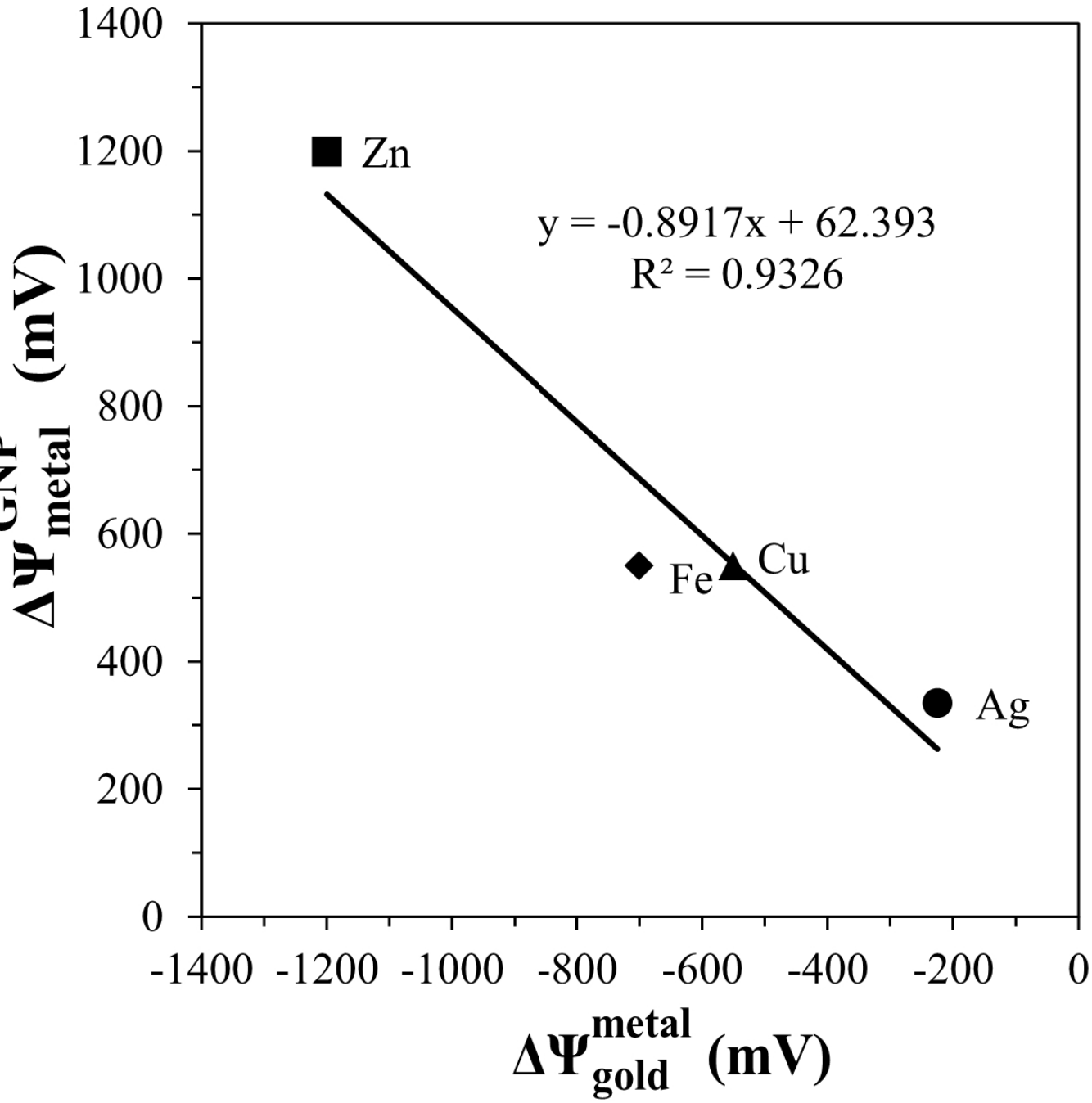
1400
1200
1000
800
600
400
200
0
-1400
-1200
-1000
-800
-600
-400
-200
0
Zn
Fe
Cu
Ag
y = -0.8917x + 62.393
R² = 0.9326
ΔΨ^GNP_metal (mV)
ΔΨ^metal_gold (mV)

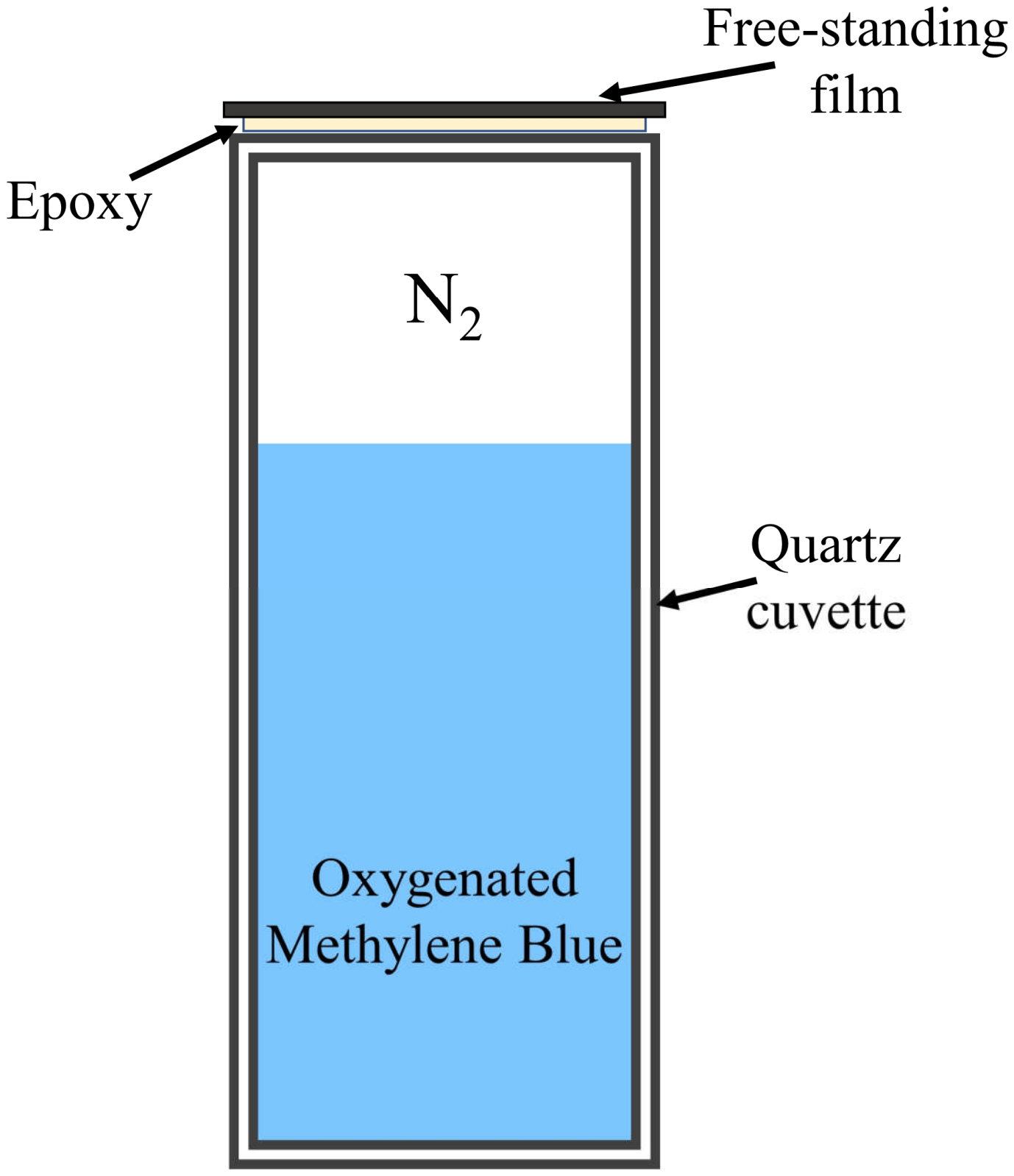
Free-standing
film
Epoxy
N_2
Quartz
cuvette
Oxygenated
Methylene Blue

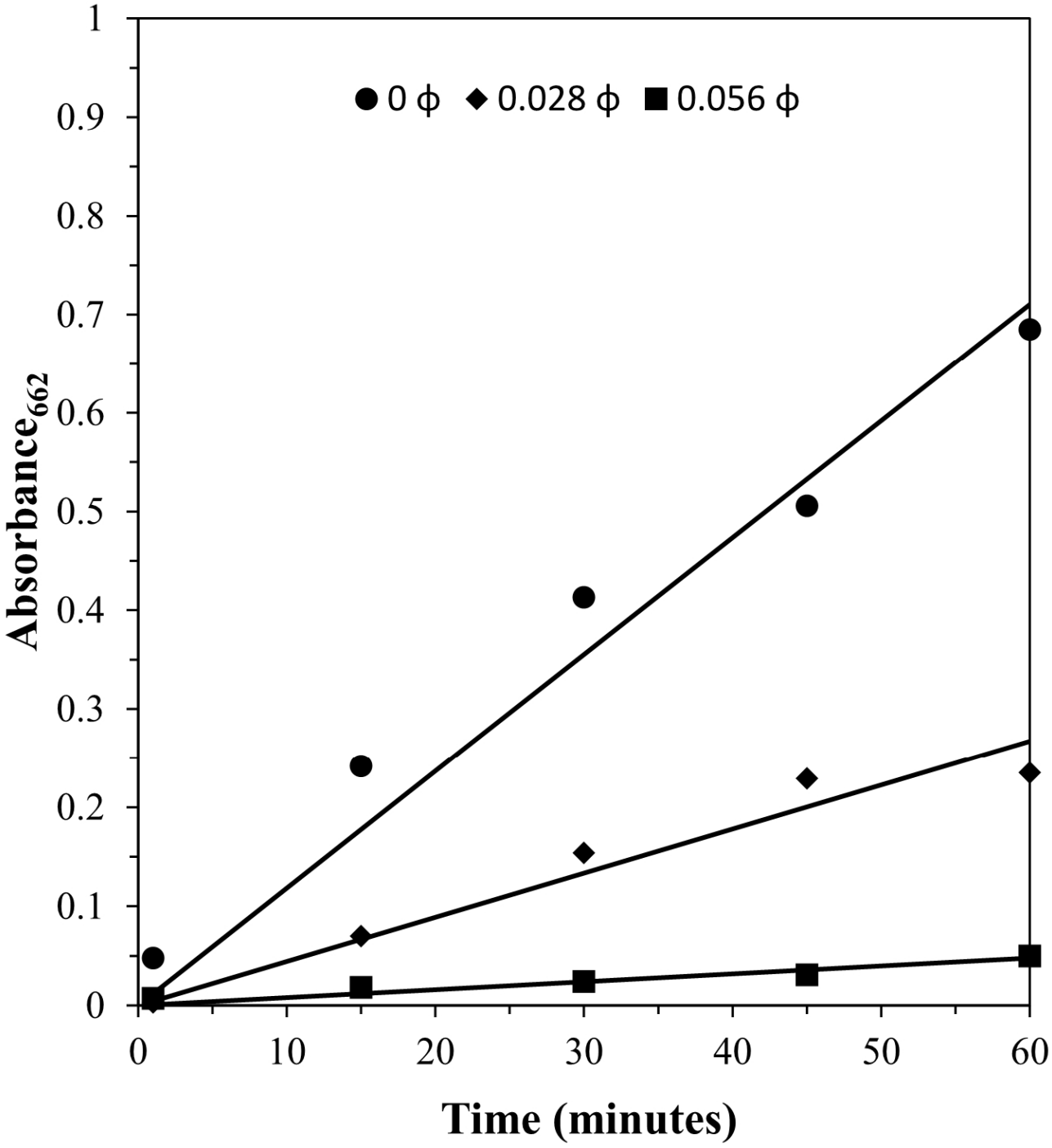
● 0 ϕ ◆ 0.028 ϕ ■ 0.056 ϕ
Absorbance662
Time (minutes)
0
0.1
0.2
0.3
0.4
0.5
0.6
0.7
0.8
0.9
1
0
10
20
30
40
50
60

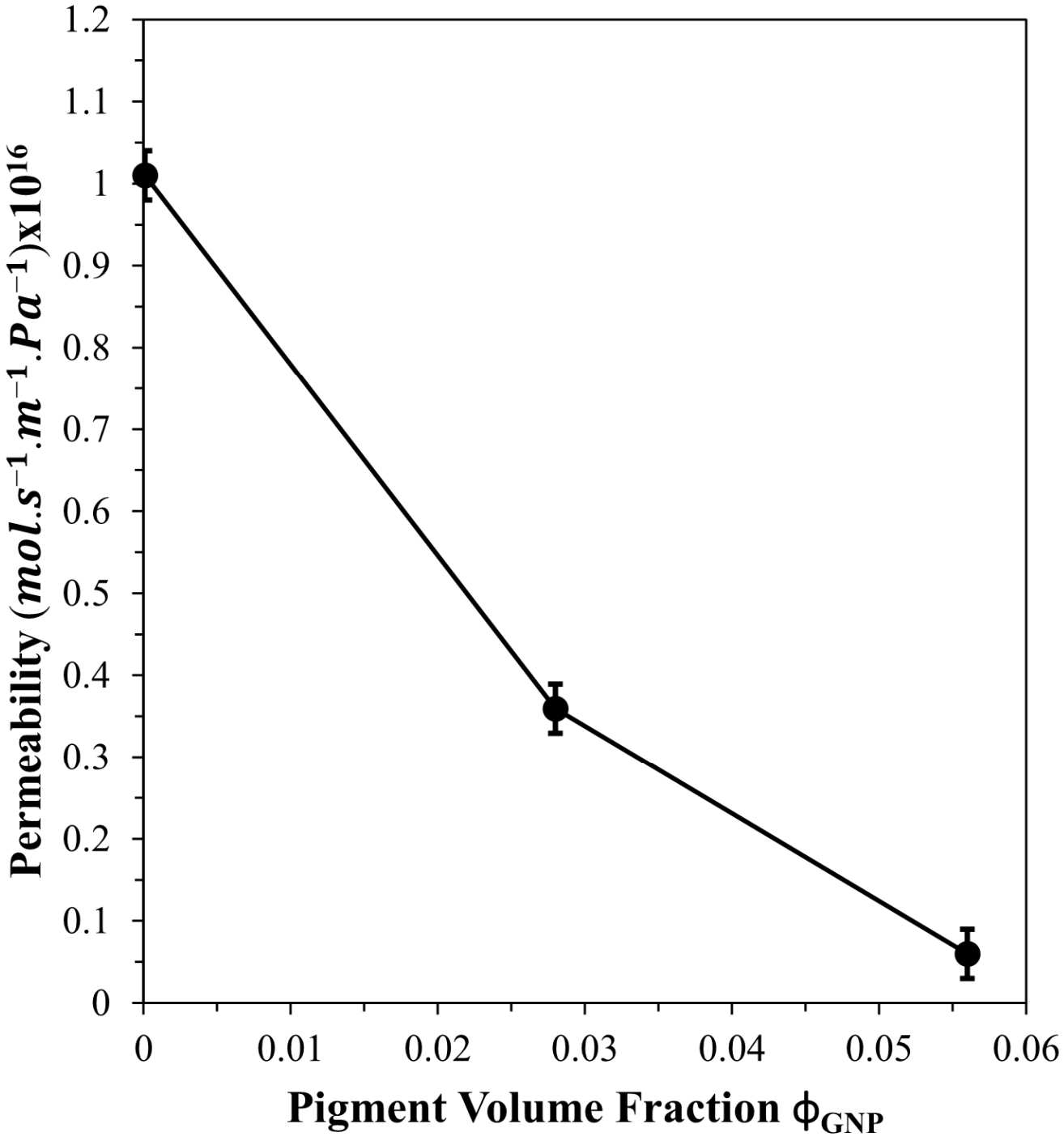
1.2
1.1
1
0.9
0.8
0.7
0.6
0.5
0.4
0.3
0.2
0.1
0
Permeability ($mol.s^{-1}.m^{-1}.Pa^{-1}$)x$10^{16}$
0
0.01
0.02
0.03
0.04
0.05
0.06
Pigment Volume Fraction ϕ_{GNP}